Detecting Tropical Forest Biomass Dynamics from Repeated LiDAR Measurements

Supplementary Material

(1) LiDAR Data Acquisition

LVIS (Laser Vegetation Imaging Sensor) is a medium altitude waveform digitizing LiDAR measuring canopy height, ground elevation, and the waveform representing the vertical profile or the distribution of intercepted surfaces within the LiDAR footprint (Hofton et al., 2002), at scan angles of ± 12º. Its expanded spatial coverage allows large scale mapping of topography, forest structure, and AGB (Weishampel et al., 2000; Drake et al., 2002a; Drake et al., 2002b). LVIS LiDAR data were collected by NASA over BCI in 1998 (Blair et al., 1999; Dubayah and Drake, 2000). This 1998 Panama LVIS survey consists of 215,984 individual LVIS shots, of which 108,184 are located over BCI and used for this study. 3077 of these shots are located over the 50 ha plot, which corresponds to an average density of 60 shots per ha, or 0.0006 shots per square meter. LVIS is flown at 1000m altitude and its large footprint (~20 m) generally exceeds the average crown diameter of large trees (King, 1996; Drake et al., 2003). LVIS accuracy has been reported to be better than 1 m (Hofton et al, 2000). Here, we consider that LVIS accuracy is less than 2m for our uncertainty analysis.

The airborne discrete-return LiDAR (DRL) that acquired data in 2009 was a small footprint instrument, ranging between 0.25m and 0.60m footprint. It is a proven technique in quantifying sub-canopy topography and providing accurate vertical forest structure (Dubayah and Drake, 2000; Hyyppa et al., 2001; Lefsky et al., 2002). The DRL

data were collected at very low altitude (between 500 and 1500m) and included repeated

passes at scan angles of ± 17º, resulting in multiple measurements per square meter (up to

10 points or echoes per square meter) for precise characterization of vegetation structure.

DRL data were collected by Blom Corporation and Northrop Grumman as part of an NSF

funded project, using an Optech 3100 LiDAR scanning at a rate of 70Khz. The data were

collected over 11 individual flights yielding a total of over 233 million laser shots, and

over 528 million individual points, resulting in an average point density of 5.6 points per

square meter (ppm^2), and 8.1 returns per square meter (rpm^2). The DRL data was post-

processed by BLOM Corporation using Bentley's MicroStation to calibrate and filter the

data. In addition to the automated filtering process, additional manual editing of the sub-

canopy DEM was performed to produce a bare-earth DEM product. To ensure accuracy

and compliance with the precision requirements, the ground surface was tested using 36

ground surveyed points on flat, hard, well defined surfaces, free of obstacles. The results

of the vertical accuracy assessment determined an average error in height of -0.069 m, an

RMSE value of 0.076 m and a standard deviation of 0.032 m. Horizontal accuracy for

similar types of DRL has been reported to be 0.1 m (Evans and Hudak, 2007). However,

we consider here that the DRL geolocation error can be higher (up to 1m) because it

depends greatly on the characteristics of the sensor and is specific to the system that is

used (GPS accuracy, flight altitude…).

Table S1 summarizes the characteristics of both sensors and highlights their differences.

Differences in footprint size and density of points have to be taken into account when

extracting and analyzing the data. In order to have a fairer comparison between the two

datasets, the DRL data was first aggregated at 20m resolution to calculate the relative

height metrics at 1 ha. Some areas are not covered by any LVIS shots, which makes it hard to compare the two surveys in these areas. At the 0.04 ha scale, 180 subplots are not covered by any LVIS shots, out of 1250. These subplots were not included in the 0.04 ha scale analysis. Geolocation errors are small (less than 1m) but they are hard to quantify. They are considered negligible at the 1 ha scale. However, they can be a source of error at smaller spatial scales, especially at 0.04 ha.

Table S1 : LVIS and DRL sensors characteristics

	LVIS	DRL
Footprint size	≈20m	0.25-60cm
altitude of flight	1000m	457.2m
scan angles	± 12°	± 17°
GPS horizontal accuracy	<1m	<1m
Density of points	$0.006ppm^2$ (50 ha plot)	$5.6ppm^2$

(2) LVIS Calibration

To compare LVIS and DRL LiDAR data for changes in vegetation structure requires the data to be cross-calibrated. We performed the cross-calibration of the sensors such that both provide the same ground elevation under forest canopy (Fricker et al., 2012). LVIS, being a large footprint LiDAR (20-25 m), has a limited ability to detect ground in dense canopy forests, particularly in complex topographies, thus affecting vegetation height metrics and potentially causing errors in AGB estimations (Dubayah et al., 2010). In contrast, the DRL sensor provides an accurate estimate of ground elevation (average error of 0.069m) and vegetation height. A shortened LVIS laser profile will result in a general underestimation of biomass and vertical stratification.

Average vertical difference between the LVIS last-return points and the DRL ground surface across BCI was of 28.7 cm. (Fricker et al, 2012). Although the majority (82.3%) of all LVIS points matched discrete return elevations to 2 meters or less, significant LVIS last-return outliers were identified, ranging from 16.4 m below the ground surface, to last-return points over 35.7 m above the ground surface across the island. Also, areas of high terrain slope show consistently more error in large-footprint LiDAR ground detection. Because our goal is to obtain optimal AGB estimations and to reduce errors due to the sensors, LVIS data had to be corrected before it was used in our AGB estimation algorithm.

LVIS data was corrected based on a method developed by Fricker et al (2012). It uses slope to correct LVIS semi-automatically. They use the LVIS sub-canopy Digital Elevation Model (DEM) alone to estimate slope and apply the effects of terrain slope on sub-canopy topography. However, for the present study we had high-resolution LiDAR data (DRL) over the whole island, so we simply used the DRL DEM as a reference for sub-canopy topography. The elevation difference between DRL and LVIS subcanopy topography was calculated for each LVIS shot by comparing the LVIS ground elevation to the DRL ground elevation in a 20m diameter circle around the center location of each shot, representing its footprint, using a nearest neighbor approach.

This difference (positive or negative) was then added to each LVIS vertical height metrics. The average difference between LVIS ground and DRL ground in the 50 ha plot was 1m ± 2.2m. The result is a more accurate LVIS digital elevation model and improved LVIS estimates of forest structure (Fig. S1), benefiting vegetation modeling applications (Evans and Hudak, 2007).
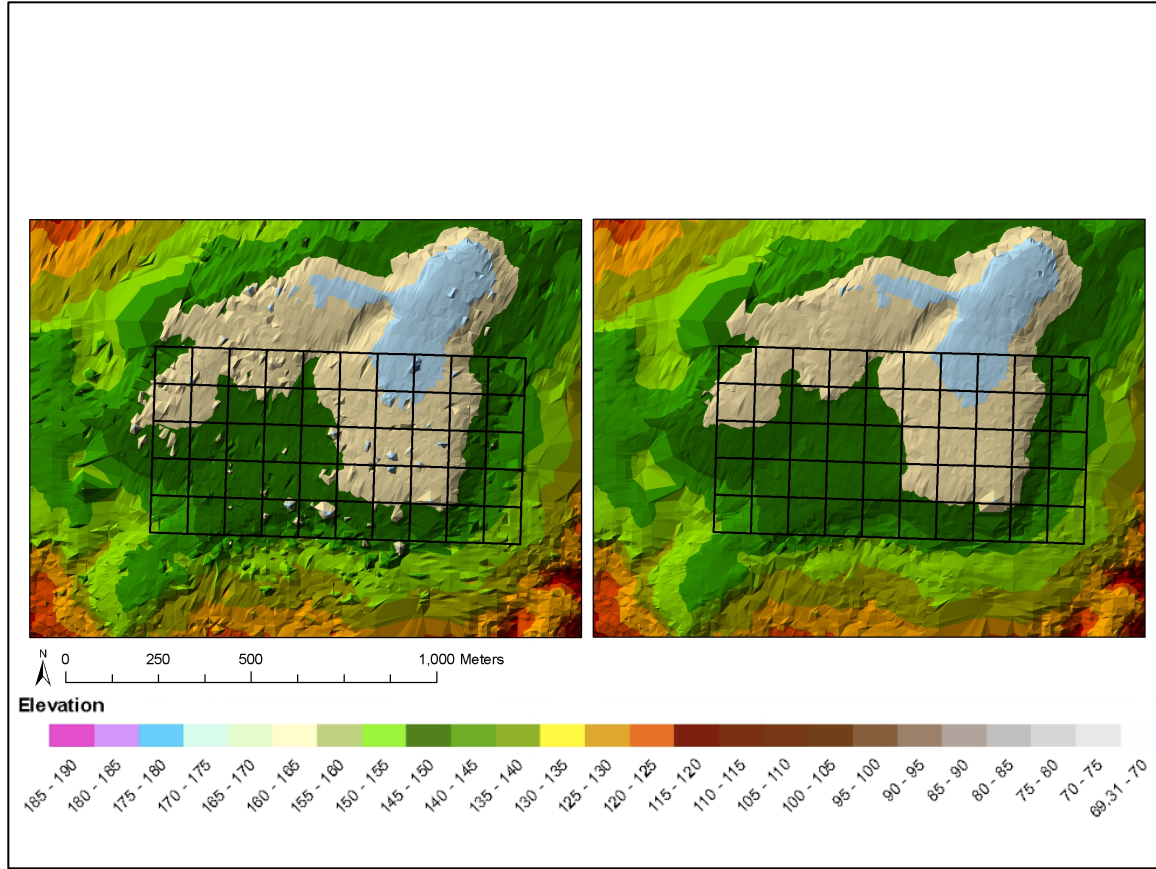
Figure S1 : LVIS ground correction. Raw LVIS ground returns (left) and corrected LVIS ground returns (right) using the DRL Digital Elevation Model.

Although the cross-calibration does not improve the relationships between LVIS and DRL intermediate metrics (RH25, RH50, RH75), it does improve $RH100_{LVIS}$ relationship to $RH100_{DRL}$ and to ground estimated AGB.

At the footprint level, correlation between $RH100_{LVIS}$ and $RH100_{DRL}$ went from $R^2 = 0.65$ to $R^2 = 0.73$ over the whole island.

At the subplot level, the relationship between $RH100_{LVIS}$ and $RH100_{DRL}$ is now closer to a one-to-one relationship, with an intercept of -1.68 and a coefficient of 1.02, versus an intercept of 4.46 and a coefficient of 0.88 without correction (1 ha subplots).

As for the relationship between LVIS metrics and Ground AGB, correlation between

RH100$_{LVIS}$ and AGB$_{2000}$ went from R^2=0.48 without correction to R^2 = 0.56 with correction.

In spite of the above corrections, DRL and LVIS present too many differences to be used the same way to estimate AGB. They do not have the same footprint size, which makes it impossible to do a proper footprint to footprint comparison to estimate AGB as done in Dubayah et al. (2010). Furthermore, LVIS height metrics were directly calculated for each shot during post-processing, whereas we calculated the DRL height metrics using the vertical histogram of canopy height for a given pixel size (at 20m, 50m and 100m resolutions).

For these reasons, intermediate height metrics are different for DRL and LVIS. LVIS intermediate height metrics are systematically lower than DRL's. RH25$_{DRL}$ >RH25$_{LVIS}$ by 9m ±2.8m), RH50$_{DRL}$ >RH50$_{LVIS}$ by 6.9m ±1.8m), RH75$_{DRL}$ >RH75$_{LVIS}$ by 5.1m ±1.3m).

As a result, our different attempts to retrieve AGB change from LiDAR by using ground estimated change (ΔAGB$_{gnd}$) and changes in RH (ΔRH) in our regression model did not show any relationship between these metrics.

Consequently, we used DRL and LVIS metrics independently in the determination of regression models for AGB estimations and proceeded in two steps : 1) estimation of AGB for both dates, 2) estimation of AGB change from these results.

(3) LiDAR Height Metrics

To develop the relative height (RH) metrics at each scale, LVIS and DRL data were extracted using shape files partitioning the 50 ha plot into respectively, 1250, 200 and 50

regions of interest representing the spatial scales of the analysis. From LVIS waveform data, relative height quartiles RH25, RH50, RH75 and RH100 were produced for each shot, where the RH100 metric represents the canopy top height or the maximum height of trees within the LiDAR footprint.

We aggregated all the shots whose center coordinates fell into a given subplot to calculate the average of the LVIS the relative height metrics (and the maximum height for RH100), rather than having their whole footprint contained in the plot, as done previously (Dubayah et al., 2010). This choice was based on the sizes of the ground subplots used in this study. Because LVIS footprint is approximately 20m, very few shots fall entirely in a 20m*20m subplot. In addition to the four relative height metrics, mean canopy height (MCH) was also extracted.

A similar approach was used to convert the canopy height data from DRL at 1 m resolution to waveforms at the same spatial scales. The relative height metrics (RH25, RH50, RH75 and RH100) were produced from these waveforms, as well as MCH. This method is therefore slightly different than the one used to retrieved LVIS metrics at each spatial scale, since only the top canopy height at 1m resolution is known for DRL.

Although the RH metrics are individually correlated (Fig. S2), using the five of them improves the R^2 and the RMSE of the ground-based AGB vs. LiDAR-based AGB. Unlike LVIS metrics that are calculated from the percentiles of energy from LVIS shots, DRL relative height metrics are directly calculated from RH100 distribution at each scale. Hence, the correlations between RH100 and the other RH metrics are higher for DRL than for LVIS (Fig. S2).
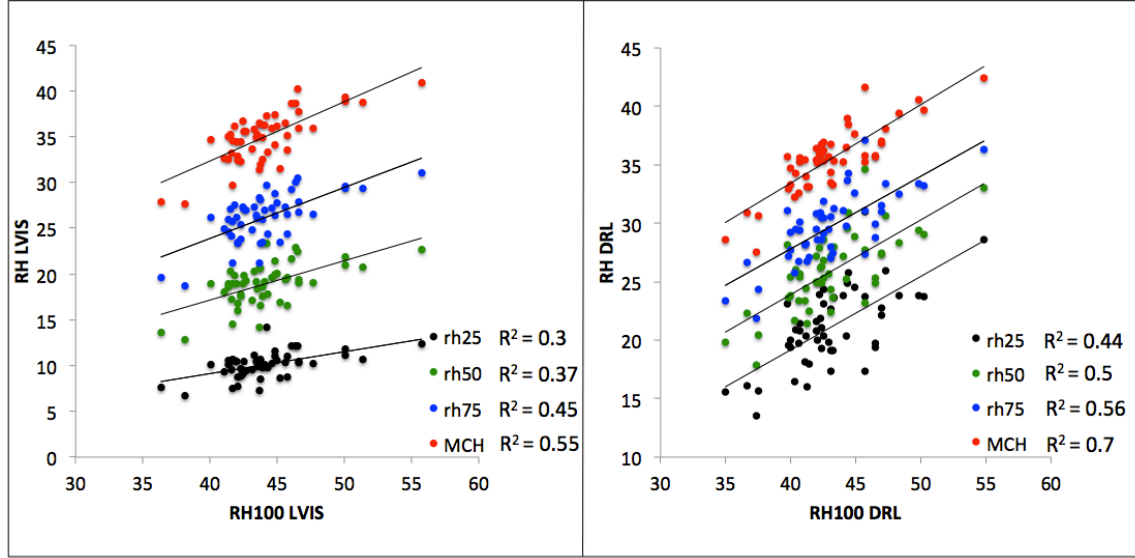
Figure S2: Relationship between the LiDAR intermediate height metrics and the maximum height of the canopy derived at 1 ha. Height metrics are correlated ($R^2 > 0.3$), but with significant variations that allow all five metrics to contribute to the biomass estimation.

(4) AGB estimation from ground measurements

Aboveground biomass density was estimated using an allometric regression model for moist tropical forests (Chave et al., 2005). The allometric method is based on the argument that the total aboveground biomass (AGB, in kg) of a tree with diameter D, measured at the breast height (DBH) 1.3m above ground must be proportional to the product of wood specific gravity (ρ) and tree stem volume. Stem volume, in turn, is proportional to the product of stem basal area and total tree height (H):

$$AGB = \exp[-2.977 + \ln(\rho D^2 H)] \cong 0.0509 \times \rho D^2 H \qquad \text{Eq. S1}$$

Where $\cong$ represents the mathematical identity meaning both formulas can be used in biomass estimation procedure. In the above equation, D (in cm) is measured during the inventory census periods, ρ (in g/cm^2) is provided from an available table of measurements for 123 species available in BCI, and tree height H is in m. Tree height

measurements were not available for all the trees in the 50 ha plot, so we developed a relationship between DBH and height of 1835 trees among them 1604 trees with DBH> 10 cm, representing 154 species (Fig S3). The equation is provided in the log form for the entire range after testing different fits to the data with different DBH ranges:

$$H = -11.731 + 22.766 \log(D), D > 10cm \qquad\qquad \text{Eq. S2}$$

We then used the height estimations as estimated from equation (ES2) into equation (ES1) for AGB estimation.
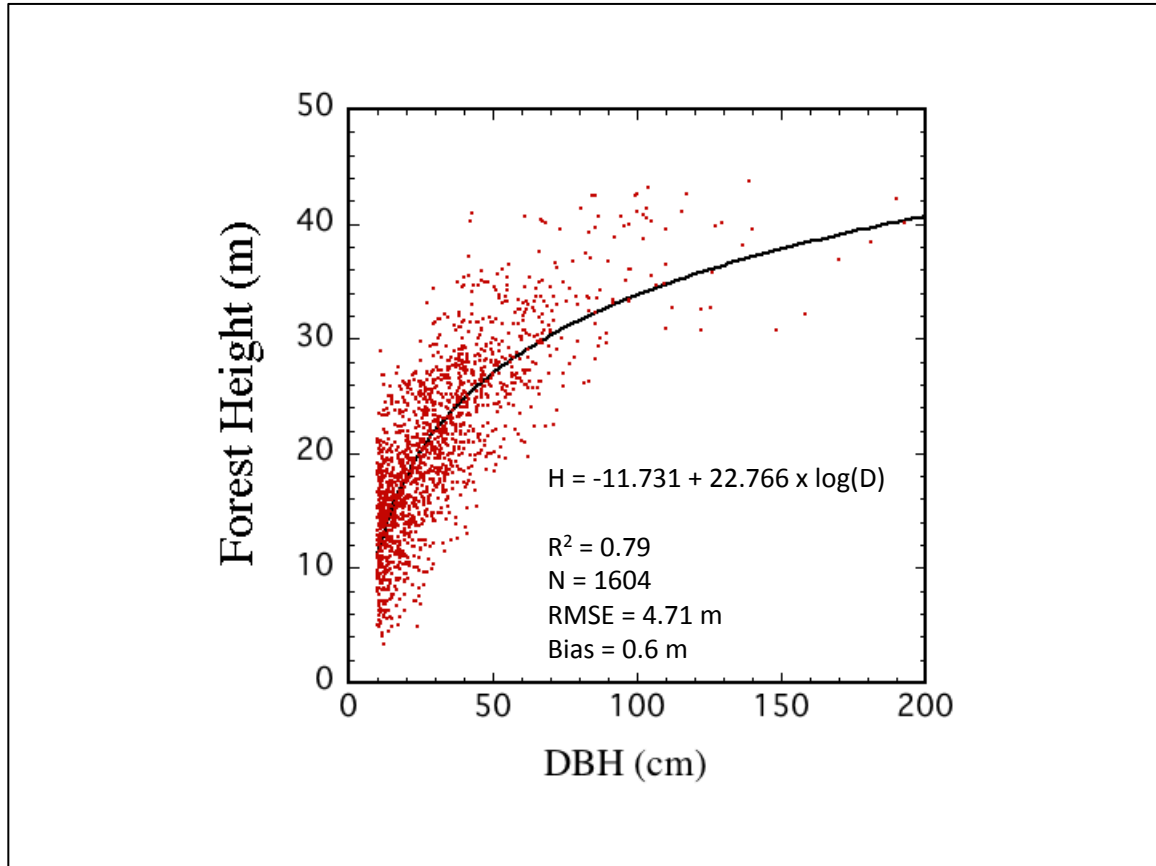

Figure S3 : Relationship between DBH (cm) and tree height H (in m).

The census data was filtered for anomalous and erroneous DBH measurements by first identifying all trees with growth larger than 45 mm/year and less than -5 mm/yr. The

DBH of these trees were replaced using growth rates equal to mean growth rate of trees in the same DBH class (Condit et al. 1993, 1999). The approach was extended to 2000, 2005, and 2010 when estimating biomass and biomass change from ground data. See Chave et al., (2003) for more details on census data trimming procedures. AGB density was then calculated for each subplot (Table S2).

Table S2 : Ground Estimated AGB in 2000, 2005 and 2010 in 1 ha subplots. The number of trees above 10cm DBH, basal area, and AGB are presented.

plot id	2000			2005			2010		
	N00	BA00	AGB00	N05	BA05	AGB05	N10	BA10	AGB10
1	679	24.50	175.00	736	25.16	173.84	726	25.48	170.33
2	625	31.84	234.97	615	31.77	236.22	590	31.29	234.71
3	600	37.17	273.48	600	38.34	284.68	594	37.49	275.34
4	631	32.25	241.86	675	31.72	234.58	712	32.09	236.92
5	578	36.13	287.76	600	35.34	282.36	630	35.75	287.70
6	676	41.00	319.02	666	41.15	324.95	659	41.65	332.91
7	735	38.81	322.66	783	36.95	308.79	742	36.52	298.18
8	750	36.86	324.15	764	37.25	333.24	755	36.76	328.61
9	668	31.58	230.80	701	32.00	235.97	683	31.51	228.99
10	699	27.49	216.05	727	25.96	196.08	788	27.09	203.27
11	675	29.53	214.24	684	29.99	222.54	646	29.69	223.13
12	691	27.68	195.43	665	26.50	181.68	704	26.05	176.53
13	676	32.04	254.21	663	30.58	238.54	664	31.39	247.34
14	622	28.51	215.91	615	28.69	222.36	608	29.20	225.91
15	686	26.83	196.29	668	27.52	202.35	665	26.55	194.40
16	642	32.91	257.96	665	32.25	254.37	618	30.33	228.90
17	703	36.55	284.99	677	33.96	259.27	688	34.20	260.67
18	668	30.82	246.19	716	31.22	249.39	744	32.14	253.53
19	722	36.87	321.76	723	36.91	324.40	696	32.91	274.80
20	600	26.10	180.53	648	27.00	187.74	657	29.34	220.85
21	761	29.51	226.48	791	28.78	224.65	811	27.41	191.91
22	681	31.23	242.24	737	31.71	248.52	715	30.96	240.71
23	623	26.87	201.48	641	26.51	198.01	636	27.24	200.68
24	484	29.92	278.06	507	30.23	286.48	516	27.81	250.36
25	512	30.12	255.78	537	26.97	211.44	574	28.70	218.27
26	686	33.98	316.98	737	33.26	311.15	706	31.70	291.37
27	706	33.32	256.59	720	34.18	266.29	725	34.21	263.54
28	643	31.45	245.74	656	30.58	232.94	674	31.53	248.54
29	737	37.01	342.30	769	36.92	347.25	764	35.96	341.34

30	732	31.69	255.71	725	32.55	264.64	735	30.97	246.13
31	837	22.40	129.86	776	22.22	129.11	773	20.67	116.14
32	681	29.10	235.44	665	27.87	222.85	619	27.62	222.12
33	693	25.59	182.73	703	25.89	183.52	722	24.82	171.58
34	679	24.10	172.68	686	23.78	169.53	693	23.25	160.55
35	641	30.42	241.19	633	29.48	238.33	651	27.97	219.34
36	578	36.69	302.60	592	36.87	309.28	606	37.64	314.00
37	717	27.94	203.51	754	27.93	203.64	748	27.13	188.36
38	634	32.53	268.01	641	32.49	272.43	656	30.02	237.33
39	776	33.67	255.18	821	33.62	259.47	827	33.36	254.91
40	805	31.69	231.88	845	31.25	229.13	859	30.79	224.54
41	802	30.61	205.98	767	28.81	189.41	793	27.42	176.61
42	834	30.43	222.48	788	29.03	213.28	763	29.04	212.33
43	863	27.27	178.60	841	27.04	177.22	896	26.40	173.06
44	752	26.26	187.53	781	25.41	178.99	805	29.26	224.67
45	714	31.33	251.18	721	29.82	245.84	727	29.24	238.80
46	716	29.76	212.86	745	28.00	198.99	733	27.12	192.87
47	860	27.86	172.76	892	28.64	181.41	830	29.27	189.26
48	749	30.76	249.56	734	31.32	255.26	761	32.27	264.93
49	735	42.38	404.06	726	41.53	398.79	712	39.71	369.13
50	687	30.45	251.54	696	30.58	255.36	696	28.87	236.20

(5) Ground estimated AGB and relative height metrics

The relationships between ground estimated AGB and the relative height metrics from both sensors have been carefully analyzed. Their correlation increases as the spatial scale becomes coarser (Fig. S4).
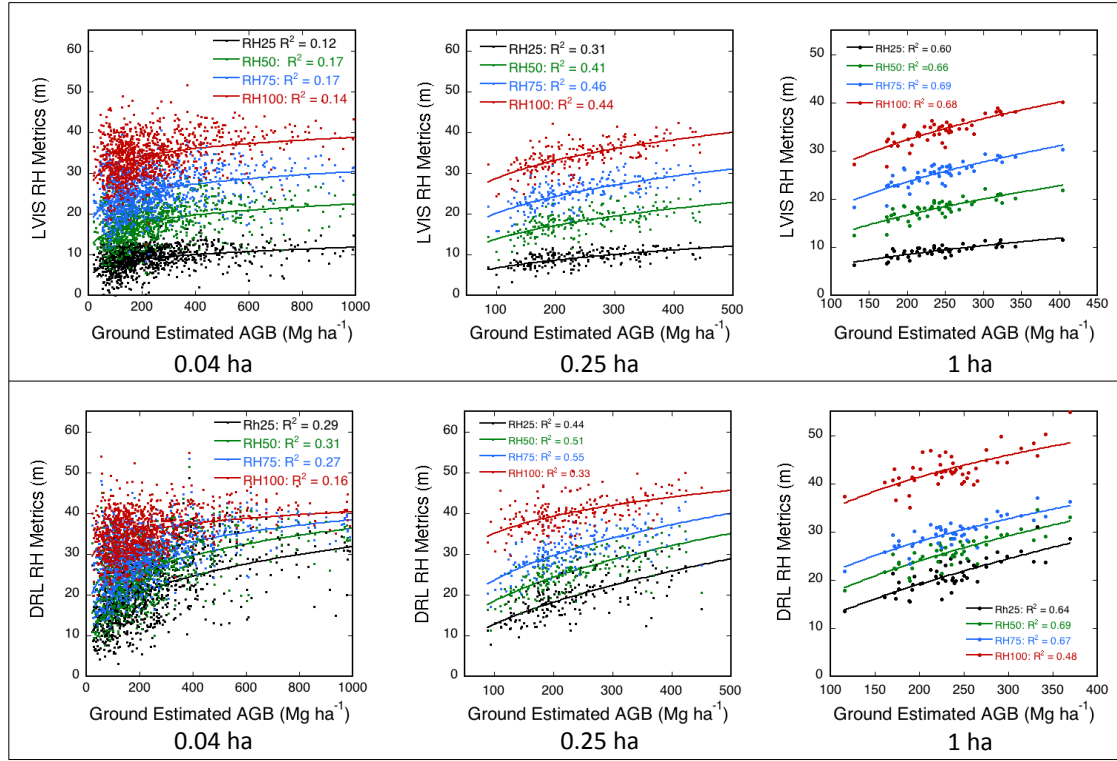
Figure S4 : Relationship between Ground Estimated AGB and RH metrics at three spatial scales (top : LVIS, bottom : DRL)

Table S3 : Coefficients of the LiDAR derived AGB equation using five height metrics at 1 ha.

$$AGB_{est} = a0 + a1RH25^{\alpha} + a2RH50^{\beta} + a3RH75^{\gamma} + a4MCH^{\delta} + a5RH100^{\varepsilon}$$

	a0	a1	a2	a3	a4	a5
LVIS 100m	-53.91	3.82	-1.03	0.46	0.05	0.02
DRL 100m	-23.8	-1.94	4.5	-1	0.08	0.05

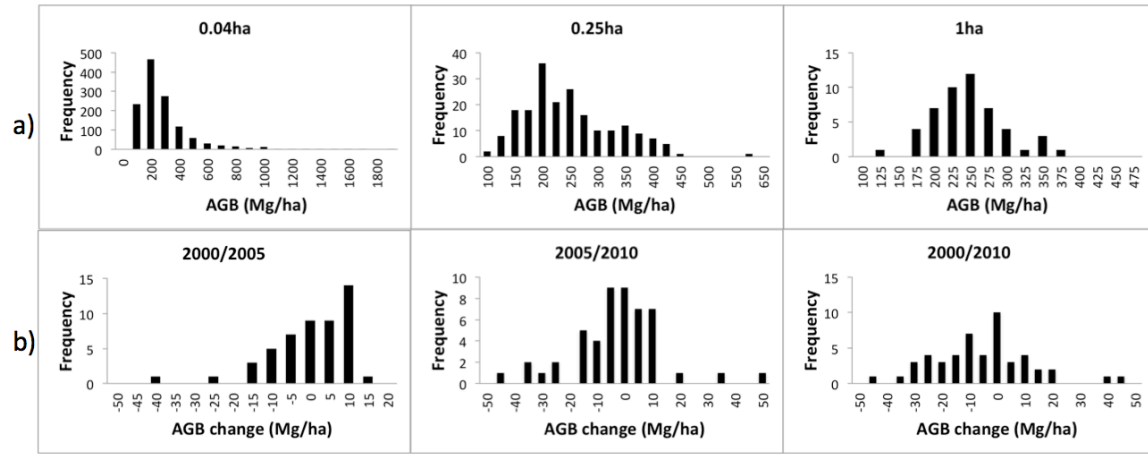|	α	β	γ	δ	ε
LVIS 100m	1.08	1.31	1.63	2.14	2.2
DRL 100m	1.06	1.42	1.74	2.14	1.8

(6) Ground-estimated AGB change

Figure S5 : a) Histograms of AGB distribution in the permanent plot at three spatial scales in 2010. AGB distribution is skewed to the left when using 0.04 ha subplots. AGB distribution becomes normal when working with larger subplots, especially at 1 ha. b) Histograms of AGB Change between 2000, 2005 and 2010 in the 50 ha plot (1 ha scale). There are more extreme values between 2005 and 2010, than between 2000 and 2005.

(7) Ground estimated AGB and MCH-derived AGB

Figure S6 shows the relationship between ground estimated AGB and LiDAR estimated AGB, using MCH only (see Fig.5 in the main paper for the 5RH approach results). The coefficients of correlation are high at 1 ha, but bias is higher than when using five relative height metrics in the model, especially as the spatial scale becomes finer.
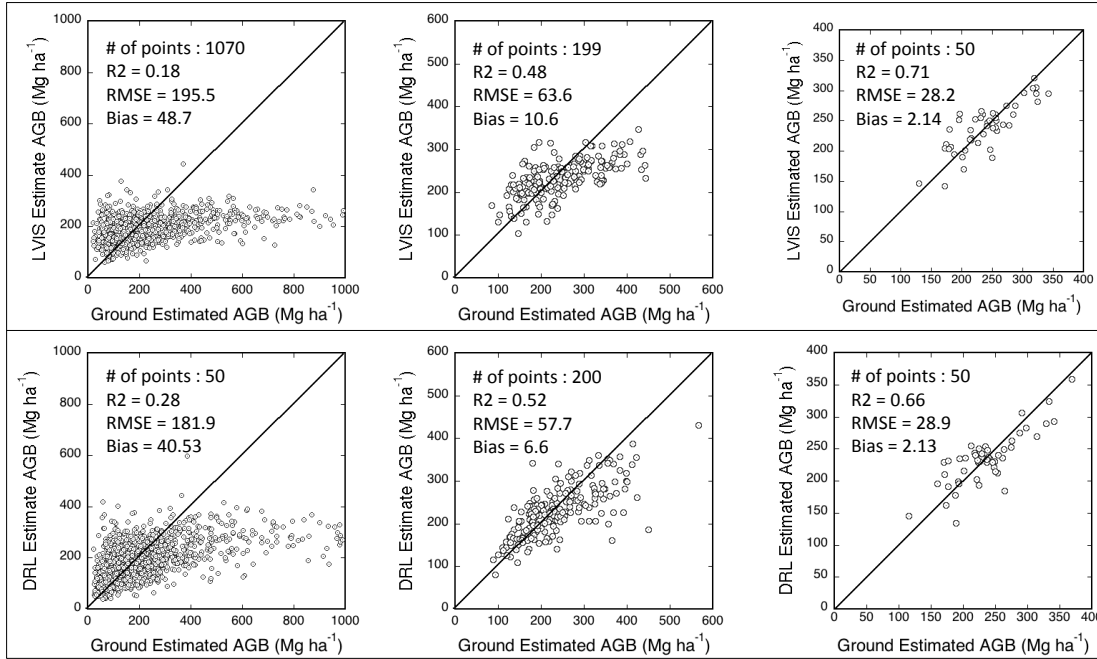
Figure S6 : Relationship between Ground estimated AGB and LiDAR estimated AGB (MCH model) (top : LVIS, bottom : DRL).

(8) Spatial Scale

Figure S7 illustrates why using small plots for estimating AGB in tropical forests may result in an improper AGB estimation. Because tree crowns can reach over 20m in diameter, chances are that a tree crown will significantly overlap several adjacent 20m*20m subplots, thus contributing to the LiDAR signal of more than one subplot. This yields to serious problems when attempting to correlate the LiDAR signal and ground-based AGB estimations because the ground measurement of a tree (i.e., the physical location of the stem) only contributes to the AGB of a single subplot. This border effect declines as the subplot size increases to 50m*50m and 100m*100m subplots, although edge effects are still expected to be present. At 1 ha, the contribution to canopy heights from trees rooted outside the plot boundary becomes small compared to those that do not transgress the plot boundaries.
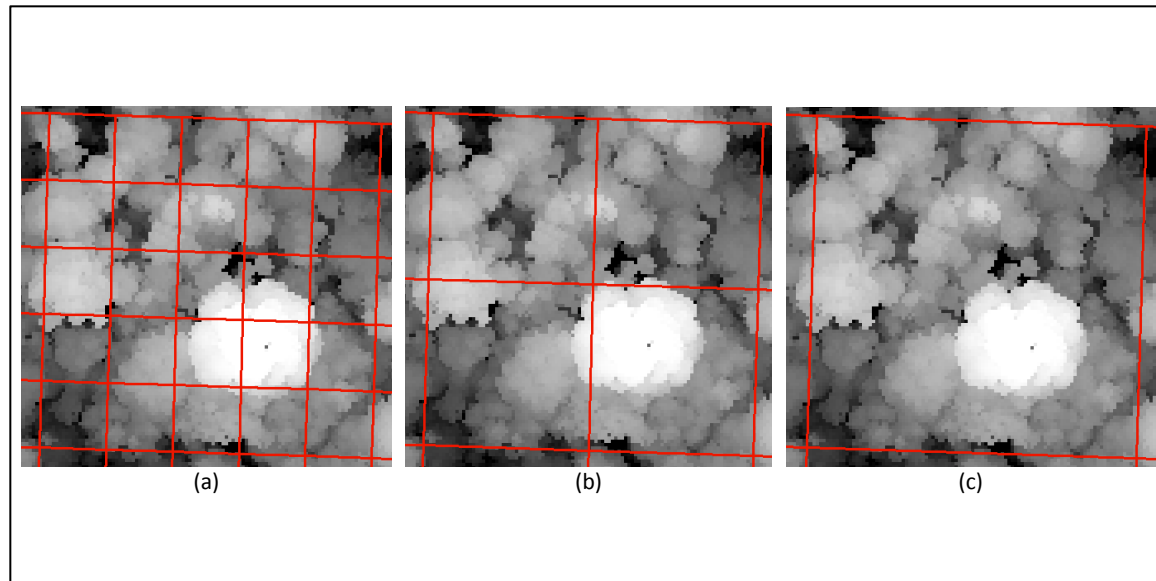
Figure S7 : Effects of plot size on DRL canopy height share. At 0.04 ha (a), a big tree is predominant in two subplots and present in two others. At 0.25 ha (b), the big tree is mainly present in one subplot, but other trees are split between subplots. At 1 ha (c), the edge effect is still there but it becomes negligible compared to the number of trees that are fully contained in the subplot.

References

Blair, J.B., Rabine, D.L., Hofton, M.A.: The Laser Vegetation Imaging Sensor: a medium-altitude, digitisation-only, airborne laser altimeter for mapping vegetation and topography. ISPRS Journal of Photogrammetry and Remote Sensing 54, 115-122, 1999.

Chave, J., Condit, R., Lao, S., Caspersen, J.P., Foster, R.B., Hubbell, S.P.: Spatial and temporal variation of biomass in a tropical forest: results from a large census plot in Panama. Journal of Ecology 91, 240-252, 2003.

Condit, R., Ashton, P.S., Manokaran, N., LaFrankie, J.V., Hubbell, S.P., Foster, R.B.: Dynamics of the forest communities at Pasoh and Barro Colorado: comparing two 50-ha plots. Philosophical Transactions of the Royal Society of London. Series B: Biological Sciences 354, 1739-1748, 1999.

Condit, R., Hubbell, S.P., Foster, R.B.: Identifying fast-growing native trees from the neotropics using data from a large, permanent census plot. Forest Ecology and Management 62, 123-143, 1993.

Dubayah, R.O., Drake, J.B.: LiDAR Remote Sensing for Forestry. Journal of Forestry 98, 44-46, 2000.

Evans, J.S., and Hudak, A.T. : A multiscale curvature algorithm for classifying discrete

return LiDAR in forested environments. IEEE Transactions on Geoscience and Remote Sensing, Vol. 45, No. 4, pp. 1029–1038, 2007.

Hofton, M. A., Blair, J. B., Minster, J.-B., Ridgway, J. R., Williams, N. P., Bufton, J. L., & Rabine, D. L.: An airborne scanning laser altimetry survey of Long Valley, California. International Journal of Remote Sensing, 21, 2413-2437, 2000.

Hofton, M.A., Rocchio, L.E., Blair, J.B., Dubayah, R.: Validation of Vegetation Canopy LiDAR sub-canopy topography measurements for a dense tropical forest. Journal of Geodynamics 34, 491-502, 2002.

Hyyppa, J., Kelle, O., Lehikoinen, M., Inkinen, M.:A segmentation-based method to retrieve stem volume estimates from 3-D tree height models produced by laser scanners. Geoscience and Remote Sensing, IEEE Transactions on 39, 969-975, 2001.

King, D.A.: Allometry and Life History of Tropical Trees. Journal of Tropical Ecology 12, 25-44, 1996.

Weishampel, J.F., Blair, J.B., Knox, R.G., Dubayah, R., Clark, D.B.: Volumetric LiDAR return patterns from an old-growth tropical rainforest canopy. International Journal of Remote Sensing 21, 409 – 415, 2000.